Nematic Ordering in the Heisenberg Spin-Glass System in d=3 Dimensions

Egemen Tunca[1] and A. Nihat Berker[2, 3, 4]

[1] TEBIP High Performers Program, Board of Higher Education of Turkey,
Istanbul University, Fatih, Istanbul 34452, Turkey
[2] Faculty of Engineering and Natural Sciences, Kadir Has University, Cibali, Istanbul 34083, Turkey
[3] TÜBITAK Research Institute for Fundamental Sciences, Gebze, Kocaeli 41470, Turkey
[4] Department of Physics, Massachusetts Institute of Technology, Cambridge, Massachusetts 02139, USA

Nematic ordering, where the spins globally align along a spontaneously chosen axis irrespective of direction, occurs in spin-glass systems of classical Heisenberg spins in $d = 3$. In this system where the nearest-neighbor interactions are quenched randomly ferromagnetic or antiferromagnetic, instead of the locally randomly ordered spin-glass phase, the system orders globally as a nematic phase. The system is solved exactly on a hierarchical lattice and, equivalently, Migdal-Kadanoff approximately on a cubic lattice. The global phase diagram is calculated, exhibiting this nematic phase, and ferromagnetic, antiferromagnetic, disordered phases. The nematic phase of the classical Heisenberg spin-glass system is also found in other dimensions $d > 2$: We calculate nematic transition temperatures in 24 dimensions in $2 < d \leq 4$.

I. INTRODUCTION: NEMATIC ORDER DUE TO QUENCHED RANDOMNESS

Spin glasses, broadly defined as systems with frozen (quenched) disorder that have locally annulling interactions (frustration), present complex systems with a plethora of distinctive characteristics. These distinctions include the spin-glass phase and its signature: chaos under repeated scale changes [1–3]. The fractal spectrum of spin-glass chaos has recently been shown to be used as a classification and clustering tool for the broadest of complex data, including multigeographic multicultural music and brain signals.[4] The ordering of the spin-glass phase has local fixation within spatial non-uniformity, the direction and magnitude of the local magnetization varying between neighboring points of a lattice, but the direction of local magnetization being firmly fixed relative to the local magnetizations of the neighbors.

The above discussion has been in terms of Ising spins, namely one-component spins, on which the preponderance of spin-glass research has been done. We find here that for three-component Heisenberg spins, the new ordering evades the directional fixation: the spins globally align along a spontaneously chosen axis irrespective of direction, thus creating a nematic spin phase. Thus, symmetry is globally broken by the spontaneous choice of a spin axis, but all local magnetizations are zero.

II. THE MODEL AND THE GENERAL METHOD

The classical Heisenberg spin-glass system is defined by the Hamiltonian

$$- \beta \mathcal{H} = \sum_{\langle ij \rangle} J_{ij} \, \vec{s}_i \cdot \vec{s}_j, \qquad (1)$$

where $\beta = 1/k_B T$, $J_{ij} = +|J|$ or $-|J|$ (ferromagnetic or antiferromagnetic) with probability p and $1 - p$ respectively, the classical spin $\vec{s}_i$ is the unit spherical vector
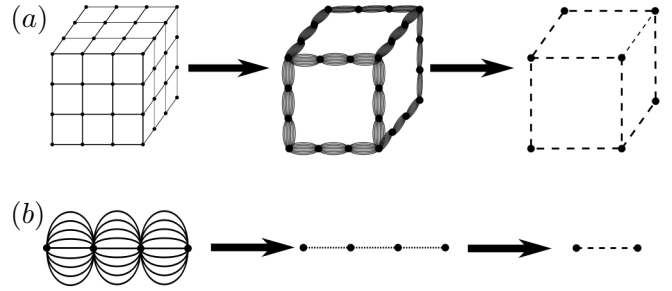

FIG. 1. (a) Migdal-Kadanoff approximate renormalization-group transformation for the $d = 3$ cubic lattice with the length-rescaling factor of $b = 3$. In this intuitive approximation, bond moving is followed by decimation. (b) Exact renormalization-group transformation of the $d = 3, b = 3$ hierarchical lattice for which the Migdal-Kadanoff renormalization-group recursion relations are exact. The construction of a hierarchical lattice proceeds in the opposite direction of its renormalization-group solution. From [7, 41].

at lattice site i, and the sum is over all nearest-neighbor pairs of sites.

We solve the classical Heisenberg spin glass by a renormalization-group transformation that is exact on the $d = 3$ hierarchical lattice and, equivalently, Migdal-Kadanoff approximate [5, 6] on the $d = 3$ cubic lattice (Fig. 1). The latter much-used approximation is physically intuitive: In a hypercubic lattice where an exact renormalization-group transformation cannot be applied, as an approximation some of the bonds are removed, which weakens the connectivity of the system and, to compensate, for every bond removed, a bond is added to the remaining bonds. This step is the bond-moving step and constitutes the approximate step of the renormalization-group transformation. At this point, the intermediate sites can be eliminated by an exact integration over their spin values in the partition function, which yields the renormalized interaction between the remaining sites. This is called the (exact) decimation step and

completes the renormalization-group transformation. As shown in Fig. 1, the renormalization-group recursion relations of the Migdal-Kadanoff approximation are identical to those of an exact solution of a hierarchical lattice [7–9]. For recent works using hierarchical lattices, see [10–22]
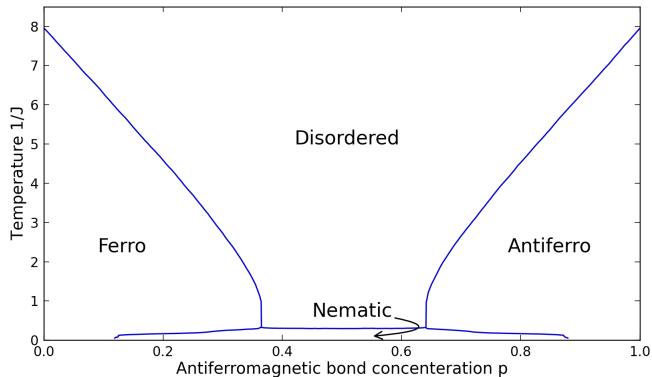

FIG. 2. Calculated phase diagram of the classical Heisenberg spin-glass system in $d = 3$. The phase diagram shows no spin-glass phase, but at low temperatures an extended nematic phase where the spins globally align along a spontaneously chosen axis irrespective of direction.

This simple renormalization-group transformation has been widely successful on different systems: the lower-critical dimension d_c below which no ordering occurs has been correctly determined as $d_c = 1$ for the Ising model [5, 6], $d_c = 2$ for the XY [23, 24] and Heisenberg [25] models, and the presence of an algebraically ordered phase has been seen for the XY model [18, 23, 24]. In q-state Potts models, the number of states q_c for the changeover from second-order to first-order phase transitions has been correctly obtained in $d = 2$ and 3.[26] In systems with frozen microscopic disorder (quenched randomness), $d_c = 2$ has been determined for the random-field Ising [27, 28] and XY models [29], and the non-integer value of $d_c = 2.46$ for the Ising spin-glass [30–36]. Also under the Migdal-Kadanoff approximation, the chaotic nature of the Ising spin-glass phases [1–3] has been obtained and Lyapunov exponentwise quantitatively analyzed, both for quenched randomly mixed ferromagnetic-antiferromagnetic spin glasses [37–39] and right- and left-chiral (helical) spin glasses [40–42].

III. MIGDAL-KADANOFF RENORMALIZATION GROUP FOR THE HEISENBERG MODEL WITH NON-UNIFORM INTERACTIONS

The algebra of the Migdal-Kadanoff transformation for discrete spin systems such as Ising, Potts, and clock models is quite simple. The transformation for the three-component classical Heisenberg model, with each spin having two continuously varying sterangles, has only

been recently achieved [25], for systems without randomness, and is not simple. Here we generalize this renormalization-group transformation to quenched random systems.
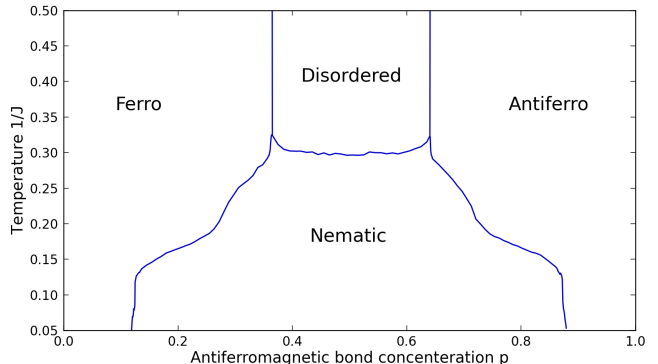

FIG. 3. Low-temperature portion of the calculated phase diagram of the classical Heisenberg spin-glass system in $d = 3$. As more fully seen here, the phase diagram shows no spin-glass phase, but at low temperatures an extended nematic phase where the spins globally align along a spontaneously chosen axis irrespective of direction.

In the first, bond-moving, step (Fig.1) of the Migdal-Kadanoff transformation,

$$\tilde{u}_{i'j'}(\gamma) = u_{i_1 j_1}(\gamma) u_{i_2 j_2}(\gamma), \qquad (2)$$

where $u_{ij}(\gamma) = e^{-\beta \mathcal{H}_{ij}(\vec{s}_i, \vec{s}_j)}$ is the exponentiated nearest-neighbor Hamiltonian between sites (i, j) and γ is the angle between the spherical unit vectors $(\vec{s}_i, \vec{s}_j)$. The tilda denotes bond-moved. Using the Fourier-Legendre series,

$$u_n(\gamma) = \sum_{l=0}^{\infty} \lambda_l^{(n)} P_l(\cos(\gamma)), \qquad (3)$$

where n denotes $i_n j_n$, with the expansion coefficient $\lambda_l^{(n)}$ evaluated as

$$\lambda_l^{(n)} = \frac{2l + 1}{2} \int_{-1}^{1} u_n(\gamma) P_l(\cos(\gamma)) \, d(\cos(\gamma)). \quad (4)$$

Thus, for the left side of Eq.(2),

$$\tilde{\lambda}_l^{(n')} = \frac{2l + 1}{2} \int_{-1}^{1} u_{n_1}(\gamma) u_{n_2}(\gamma) P_l(\cos \gamma) \, d(\cos \gamma) =$$

$$\frac{2l + 1}{2} \sum_{l_1=0}^{\infty} \sum_{l_2=0}^{\infty} \lambda_{l_1}^{(n_1)} \lambda_{l_2}^{(n_2)} \cdot$$

$$\int_{-1}^{1} P_{l_1}(\cos \gamma) P_{l_2}(\cos \gamma) P_l(\cos \gamma) \, d(\cos \gamma)$$

$$= \sum_{l_1=0}^{\infty} \sum_{l_2=0}^{\infty} \lambda_{l_1}^{(n_1)} \lambda_{l_2}^{(n_2)} \langle l_1 l_2 00 | l_1 l_2 l 0 \rangle^2, \quad (5)$$

where the bracket notation is the Clebsch-Gordan coefficient with the restrictions $l_1 + l_2 + l = 2s, s \in \mathbf{N}$; $|l_1 - l_2| \le l \le |l_1 + l_2|$.

In the second, decimation, step of the Migdal-Kadanoff transformation, a decimated bond is obtained by integrating over the shared spin of two bonds,

$$u'_{13}(\gamma_{13}) = \int \tilde{u}_{12}(\gamma_{12})\tilde{u}_{23}(\gamma_{23})\frac{d\vec{s}_2}{4\pi} =$$
$$= \sum_{l_1=0}^{\infty}\sum_{l_2=0}^{\infty}\int \tilde{\lambda}_{l_1}^{(n_1)}\tilde{\lambda}_{l_2}^{(n_2)}P_{l_1}(\cos\gamma_{12})P_{l_2}(\cos\gamma_{23})\frac{d\vec{s}_2}{4\pi}. \quad (6)$$

The prime denotes renormalized. Expressing the Legendre polynomials in terms of spherical harmonics,

$$= \sum_{l_1=0}^{\infty}\sum_{l_2=0}^{\infty}\sum_{m_1=-l_1}^{l_1}\sum_{m_2=-l_2}^{l_2}\tilde{\lambda}_{l_1}^{(n_1)}\tilde{\lambda}_{l_2}^{(n_2)}\frac{(4\pi)^2}{(2l_1+1)(2l_2+1)} \cdot$$
$$\int Y_{l_1}^{m_1}(\vec{s}_1)Y_{l_1}^{m_1*}(\vec{s}_2)Y_{l_2}^{m_2}(\vec{s}_2)Y_{l_2}^{m_2*}(\vec{s}_3)\frac{d\vec{s}_2}{4\pi}, \quad (7)$$

evaluating the integral and summing over the resulting delta functions,

$$= \sum_{l_1=0}^{\infty}\sum_{m_1=-l_1}^{l_1}\tilde{\lambda}_{l_1}^{(n_1)}\tilde{\lambda}_{l_1}^{(n_2)}\frac{4\pi}{(2l_1+1)^2}Y_{l_1}^{m_1}(\vec{s}_1)Y_{l_1}^{m_1*}(\vec{s}_3), \quad (8)$$

due to occcuring Dirac delta functions. Rearranging the spherical harmonics back to Legendre polynomials and combining with Eq.(5),

$$\lambda_l^{(n')} = \frac{1}{(2l+1)}\Big(\sum_{l_1=0}^{\infty}\sum_{l_2=0}^{\infty}\lambda_{l_1}^{(n_1)}\lambda_{l_2}^{(n_2)}\langle l_1 l_2 00|l_1 l_2 l0\rangle^2\Big) \cdot$$
$$\Big(\sum_{l_3=0}^{\infty}\sum_{l_4=0}^{\infty}\lambda_{l_3}^{(n_3)}\lambda_{l_4}^{(n_4)}\langle l_3 l_4 00|l_3 l_4 l0\rangle^2\Big), \quad (9)$$

the full recursion relations of the renormalization-group are obtained. The bond-moved $\tilde{\lambda}$ were substituted from Eq.(5). Thus, the renormalization-group transformation is in terms of the Fourier-Legendre coefficients $\lambda_l^{(n')}(\{\lambda_l^{(n_i)}\})$. We have kept up to $l = 25$ in our numerical calculations of the trajectories.

IV. MIGDAL-KADANOFF RENORMALIZATION GROUP FOR THE HEISENBERG MODEL WITH QUENCHED RANDOMNESS

Having derived the renormalization-group transformation for non-uniform nearby interactions, we can now proceed with the solution of the quenched random problem of the spin-glass Heisenberg system in d dimensions,
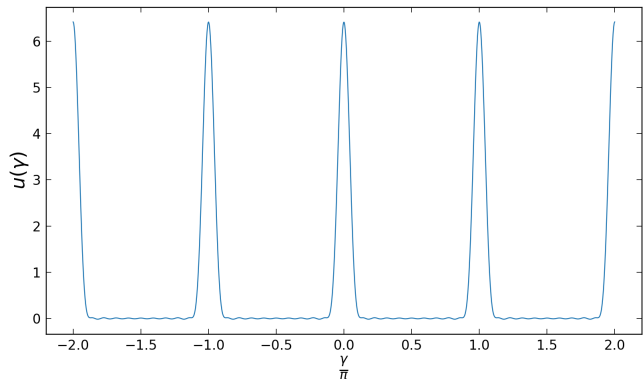

FIG. 4. The fixed-point exponentiated potential $u(\gamma)$ at the renormalization-group sink of the nematic phase. The neighboring spins align (nearest-neighbor angle $\gamma = 0$) or anti-align ($\gamma = \pi$), creating the nematic phase with a global spontaneous alignment axis along which both spin directions occur. All points in the nematic phase flow, under repeated renormalization-group transformations, to this sink which epitomizes the ordering of this phase. This potential function, in terms of the nearest-neighbor angle γ, is reconstructed from the Fourier-Legendre coefficients at the renormalization-group sink.

exactly on hierarchical lattices and Migdal-Kadanoff approximately on hypercubic lattices. We start with 30,000 local ferromagnetic and antiferromagnetic interactions as dictated by the antiferromagnetic probability p given after Eq.(1). We randomly select from this group to generate 30,000 new interactions. Remembering that for each interaction, 25 Fourier-Legendre coefficients are kept, this is a gigantic calculation. In order to conserve the ferromagnetic-antiferromagnetic symmetry of the system, the length rescaling factor of $b = 3$ is chosen. In the bond-moving step, b^{d-1} interactions are moved onto one interaction. In the decimation step, b interactions in series are decimated into one.

The renormalization-group trajectories (of sets of 30,000 interactions) are effected by repeated applications of the above transformation. The initial points of these trajectories are obtained from the Hamiltonian in Eq.(1), which can be written as

$$-\beta\mathcal{H} = \sum_{<ij>}J_{ij}\vec{s}_i \cdot \vec{s}_j = \sum_{<ij>}J_{ij}\cos\gamma_{ij}. \quad (10)$$

Using the plane-wave expansion for the term in the partition function involving the two spins,

$$e^{J\cos\gamma} = \sum_{l=0}^{\infty}(2l+1)i^l j_l(-iJ)P_l(\cos\gamma) = \sum_{l=0}^{\infty}\lambda_l P_l(\cos\gamma), \quad (11)$$

where $j_l(-iJ)$ is a spherical Bessel function and $P_l(\cos\gamma)$ is a Legendre polynomial.

With no approximation, after every decimation and after setting up the initial conditions, the coefficients $\{\lambda_l\}$ are divided by the largest λ_l. This is equivalent to sub-

tracting a constant term from the Hamiltonian and prevents numerical overflow problems in flows inside the ordered phases.

V. NEMATIC PHASE: GLOBAL ALIGNMENT SPONTANEOUSLY GENERATED FROM SPIN-GLASS DISORDER

Under repeated applications of the renormalization-group transformation of Eq.(9), the Fourier-Legendre coefficients flow to a stable fixed point, which is the sink of a thermodynamic phase. The sinks of the disordered phase and the ferromagnetic phase have been discussed and analyzed elsewhere [25]. The sink of the antiferromagnetic phase is identical to the sink of the ferromagnetic phase, except that the sharp central peak is at nearest-neighbor angle $\gamma = \phi$.
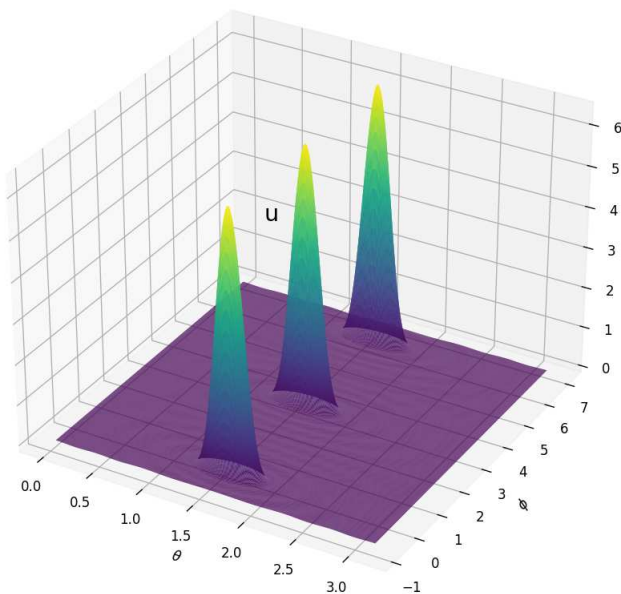

FIG. 5. The fixed-point exponentiated potential $u(\gamma)$ of the sink of the nematic phase of the $d = 3$ classical Heisenberg spin-glass system. This potential function, in terms of the spherical coordinate angles θ and ϕ of one spin with respect to the other, is reconstructed from the Fourier-Legendre coefficients at the sink.

For $d = 3$ for the classical Heisenberg spin system, a new phase occurs in the low-temperature quenched-disorder region of the phase diagram, as seen in Figs. 2 and 3, where the spin-glass phase is for the Ising system. The sink of this phase is shown in Figs. 4 and 5. Fig. 4 shows, at the sink, the exponentiated nearest-neighbor Hamiltonian $u_{ij}(\gamma) = e^{-\beta \mathcal{H}_{ij}(\vec{s}_i, \vec{s}_j)}$ between sites (i,j) versus the angle γ between the spherical unit vectors $(\vec{s}_i, \vec{s}_j)$. Fig. 5 shows, at the sink, the exponentiated nearest-neighbor Hamiltonian $u_{ij}(\gamma)$ versus the angles θ and ϕ between $(\vec{s}_i, \vec{s}_j)$. It is thus seen that the neighboring spins align (nearest-neighbor angle $\gamma = 0$) or

anti-align ($\gamma = \pi$), globally creating the nematic phase, where a spontaneous alignment axis along which both spin directions occur. All points in the nematic phase flow, under repeated renormalization-group transformations, to this sink which epitomizes the global ordering of this phase.

It is seen that, in the Heisenberg spin-glass system, at low temperature, this nematic phase extends wider, from $p = 0.12$ to 0.88, as compared with the identically placed spin-glass phase of the Ising spin-glass system. A similar widening, from $p = 0.24$ to 0.76 to essentially $p = 0$ to 1 is seen [43] in the Ising spin-glass phase, when thermal vacancies are included, making domain flipping more favorable, thus eating into the ferromagnetic (and antiferromagnetic) phases without loosing order. A similar mechanism may be in effect in the present case, with the continuously varying directions of the Heisenberg spins making domain flipping more favorable.

The nematic phase of the classical Heisenberg spin-glass system is also calculated in $d = 2.26, 2.46, 2.63, 2.77, 2.89$ dimensions and in dimensions $d \geq 3$. Our calculated transition temperatures, for 24 dimensions in $2 < d \leq 4$, are shown in Fig. 6. No nematic (or ferromagnetic [25]) phase occurs in $d = 2$, which is expected.
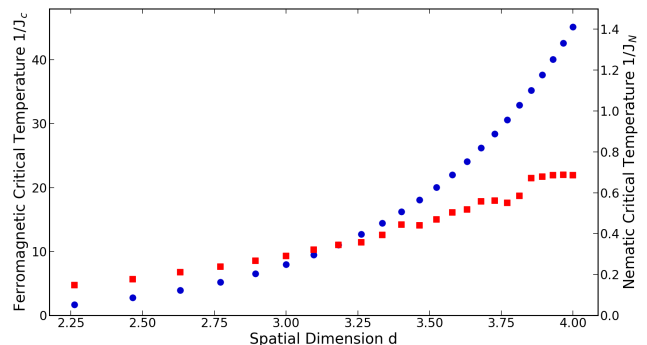

FIG. 6. Calculated transition temperatures for the nematic phase (at $p = 0.5$), squares and right vertical scale, and for the ferromagnetic phase (at $p = 1$), circles and left vertical scale, for 24 dimensions in $2 < d \leq 4$. No nematic (or ferromagnetic [25]) phase occurs in $d = 2$, which is expected.

VI. CONCLUSION

We have solved the classical Heisenberg spin-glass system by renormalization-group theory. In $d > 2$, in this system with quenched local randomness, a low-temperature phase with global order, in the form of a spontaneously chosen spin easy-axis, irrespective of spin direction. Thus, a nematic phase occurs in the Heisenberg spin system with competing ferromagnetic and antiferromagnetic interactions.

ACKNOWLEDGMENTS

[1] S. R. McKay, A. N. Berker, and S. Kirkpatrick, Spin-glass behavior in frustrated Ising models with chaotic renormalization-group trajectories, Phys. Rev. Lett. **48**, 767 (1982).

[2] S. R. McKay, A. N. Berker, and S. Kirkpatrick, Amorphously packed, frustrated hierarchical models: Chaotic rescaling and spin-glass behavior, J. Appl. Phys. **53**, 7974 (1982).

[3] A. N. Berker and S. R. McKay, Hierarchical models and chaotic spin glasses, J. Stat. Phys. **36**, 787 (1984).

[4] E.C. Artun, I. Keçoğlu, A. Türkoğlu, and A. N. Berker, Multifractal spin-glass chaos projection and interrelation of multicultural music and brain signals, arXiv:2201.10261 [cond-mat.dis-nn] (2022).

[5] A. A. Migdal, Phase transitions in gauge and spin lattice systems, Zh. Eksp. Teor. Fiz. **69**, 1457 (1975) [Sov. Phys. JETP **42**, 743 (1976)].

[6] L. P. Kadanoff, Notes on Migdal's recursion formulas, Ann. Phys. (N.Y.) **100**, 359 (1976).

[7] A. N. Berker and S. Ostlund, Renormalisation-group calculations of finite systems: Order parameter and specific heat for epitaxial ordering, J. Phys. C **12**, 4961 (1979).

[8] R. B. Griffiths and M. Kaufman, Spin systems on hierarchical lattices: Introduction and thermodynamic limit, Phys. Rev. B **26**, 5022R (1982).

[9] M. Kaufman and R. B. Griffiths, Spin systems on hierarchical lattices: 2. Some examples of soluble models, Phys. Rev. B **30**, 244 (1984).

[10] K. Jiang, J. Qiao, and Y. Lan, Chaotic renormalization flow in the Potts model induced by long-range competition, Phys. Rev. E **103**, 062117 (2021).

[11] G. Mograby, M. Derevyagin, G. V. Dunne, and A. Teplyaev, Spectra of perfect state transfer Hamiltonians on fractal-like graphs, J. Phys. A **54**, 125301 (2021).

[12] I. Chio, R. K. W. Roeder, Chromatic zeros on hierarchical lattices and equidistribution on parameter space, Annales de l'Institut Henri Poincaré D, **8**, 491 (2021).

[13] B. Steinhurst and A. Teplyaev, Spectral analysis on Barlow and Evans' projective limit fractals, J. Spectr. Theory **11**, 91 (2021).

[14] A. V. Myshlyavtsev, M. D. Myshlyavtseva, and S. S. Akimenko, Classical lattice models with single-node interactions on hierarchical lattices: The two-layer Ising model, Physica A **558**, 124919 (2020).

[15] M. Derevyagin, G. V. Dunne, G. Mograby, and A. Teplyaev, Perfect quantum state transfer on diamond fractal graphs, Quantum Information Processing, **19**, 328 (2020).

[16] S.-C. Chang, R. K. W. Roeder, and R. Shrock, q-Plane zeros of the Potts partition function on diamond hierarchical graphs, J. Math. Phys. **61**, 073301 (2020).

[17] C. Monthus, Real-space renormalization for disordered systems at the level of large deviations, J. Stat. Mech. - Theory and Experiment, 013301 (2020).

[18] O. S. Sarıyer, Two-dimensional quantum-spin-1/2 XXZ magnet in zero magnetic field: Global Thermodynamics from renormalisation group theory, Philos. Mag. **99**, 1787 (2019).

[19] P. A. Ruiz, Explicit formulas for heat kernels on diamond fractals, Comm. Math. Phys. **364**, 1305 (2018).

[20] M. J. G. Rocha-Neto, G. Camelo-Neto, E. Nogueira, Jr., and S. Coutinho, The Blume–Capel model on hierarchical lattices: Exact local properties, Physica A **494**, 559 (2018).

[21] F. Ma, J. Su, Y. X. Hao, B. Yao, and G. G. Yan, A class of vertex–edge-growth small-world network models having scale-free, self-similar and hierarchical characters, Physica A **492**, 1194 (2018).

[22] S. Boettcher and S. Li, Analysis of coined quantum walks with renormalization, Phys. Rev. A **97**, 012309 (2018).

[23] J. V. José, L. P. Kadanoff, S. Kirkpatrick, and D. R. Nelson, Renormalization, vortices, and symmetry-breaking perturbations in two-dimensional planar model, Phys. Rev. B **16**, 1217 (1977).

[24] A. N. Berker and D. R. Nelson, Superfluidity and phase separation in helium films, Phys. Rev. B **19**, 2488 (1979).

[25] E. Tunca and A. N. Berker, Renormalization-group theory of the Heisenberg model in d dimensions, arXiv:2202.06049 [cond-mat.stat-mech] (2022).

[26] H. Y. Devre and A. N. Berker, First-order to second-order phase transition changeover and latent heats of q-state Potts models in d=2,3 from a simple Migdal-Kadanoff adaptation, Phys. Rev. E **105**, 054124 (2022).

[27] M. S. Cao and J. Machta, Migdal-Kadanoff study of the random-field Ising model, Phys. Rev. B **48**, 3177 (1993).

[28] A. Falicov, A. N. Berker, and S. R. McKay, Renormalization-group theory of the random-field Ising model in 3 dimensions, Phys. Rev. B **51**, 8266 (1995).

[29] K. Akın and A. N. Berker, Lower-critical dimension of the random-field XY model and the zero-temperature critical line, arXiv:2203.11153 [cond-mat.stat-mech] (2022).

[30] S. Franz, G. Parisi, and M.A. Virasoro, Interfaces and lower critical dimension in a spin-glass Model, J. Physique I **4**, 1657 (1994).

[31] C. Amoruso, E. Marinari, O. C. Martin, and A. Pagnani, Scalings of domain wall energies in two dimensional Ising spin glasses, Phys. Rev. Lett. **91**, 087201 (2003).

[32] J.-P. Bouchaud, F. Krzakala, and O. C. Martin, Energy exponents and corrections to scaling in Ising spin glasses, Phys. Rev. B **68**, 224404 (2003).

[33] S. Boettcher, Stiffness of the Edwards-Anderson model in all dimensions, Phys. Rev. Lett. **95**, 197205 (2005).

[34] M. Demirtaş, A. Tuncer, and A. N. Berker, Lower-critical spin-glass dimension from 23 sequenced hierarchical models, Phys. Rev. E 92, 022136 (2015).

[35] A. Maiorano and G. Parisi, Support for the value 5/2 for the spin glass lower critical dimension at zero magnetic field, Proc. Natl. Acad. Sci. USA **115**, 5129 (2018).

[36] B. Atalay and A. N. Berker, A lower lower-critical spin-glass dimension from quenched mixed-spatial-dimensional spin glasses, Phys. Rev. E 98, 042125 (2018).

[37] E. Ilker and A. N. Berker, High q-state clock spin glasses in three dimensions and the Lyapunov exponents of chaotic phases and chaotic phase boundaries, Phys. Rev. E **87**, 032124 (2013).

[38] E. Ilker and A. N. Berker, Overfrustrated and underfrustrated spin glasses in d=3 and 2: Evolution of phase diagrams and chaos including spin-glass order in d=2, Phys. Rev. E **89**, 042139 (2014).

[39] E. Ilker and A. N. Berker, Odd q-state clock spin-glass models in three dimensions, asymmetric phase diagrams, and multiple algebraically ordered phases, Phys. Rev. E **90**, 062112 (2014).

[40] T. Çağlar and A. N. Berker, Chiral Potts spin glass in d = 2 and 3 dimensions, Phys. Rev. E **94**, 032121 (2016).

[41] T. Çağlar and A. N. Berker, Devil's staircase continuum in the chiral clock spin glass with competing ferromagnetic-antiferromagnetic and left-right chiral interactions, Phys. Rev. E **95**, 042125 (2017).

[42] T. Çağlar and A. N. Berker, Phase transitions between different spin-glass phases and between different chaoses in quenched random chiral systems, Phys. Rev. E **96**, 032103 (2017).

[43] G. Gülpınar and A. N. Berker, Quenched-vacancy induced spin-glass order, Phys. Rev. E **79**, 021110 (2009).